Film Morphology and Thin Film Transistor Performance of Solution-Processed Oligothiophenes

Paul C. Chang,† Josephine Lee,† Daniel Huang,† Vivek Subramanian,*,† Amanda R. Murphy,‡ and Jean M. J. Fréchet‡

Department of Electrical Engineering and Computer Sciences and Department of Chemistry, University of California, Berkeley, California 94720

Received March 1, 2004. Revised Manuscript Received June 19, 2004

The relationship between film morphology and thin film transistor (TFT) performance was investigated for two symmetrical α,ω-substituted sexithiophene derivatives containing thermally removable solubilizing groups. Solution deposition methods such as spin-coating, dip-casting, and inkjet-printing were optimized for solvent and annealing temperatures, and several substrate surface treatments were explored. The resulting thin films were characterized with AFM and the observed semiconductor performance was found to correlate with the morphology of the films, with the most crystalline films exhibiting the highest performance. Devices showed overall mobilities as high as 0.07 cm^2/V s with on/off ratios > 10^8, which are among the highest reported values for oligothiophenes solution cast at room temperature.

Introduction

Over the past decade, organic semiconducting materials have emerged as a low-cost alternative to silicon with applications in devices such as organic thin film transistors (OTFTs),[1−3] light-emitting diodes (OLEDs),[4,5] photovoltaic cells,[6] sensors,[7,8] and radio frequency identification (RF-ID) tags[9−11] for integration into low-cost, large-area electronics. Suitably modified organic materials are compatible with solution-processing techniques, thereby eliminating the need for expensive lithography and vacuum deposition steps mandatory for silicon-based materials. Low-temperature solution processing also expands the repertoire of tolerant substrates and processing options, allowing flexible plastics or fabrics to be used in conjunction with methods such as spin-coating,[3,12] stamping,[13,14] or inkjet-printing.[15,16]

One of the challenges left to address in fully integrated solution-processed organic devices lies in the inherent insolubility of the organic semiconductors offering the highest performance in OTFTs. In general, soluble semiconductors offer lower performance than their insoluble counterparts.[17−21] Functionalization required to impart solubility interrupts the natural π-stacking tendency of the molecules, which can inhibit high charge mobility that relies heavily on π-orbital overlap. To this end, we recently reported the symmetrically α,ω-ester-substituted sexithiophene derivative **EtB12T6** (Scheme 1), containing thermally removable solubilizing groups and its incorporation into solution-processed OTFTs.[22] Bulky and highly soluble ester end groups allowed the oligomers to be solution cast into thin films

* Author for correspondence. E-mail: viveks@eecs.berkeley.edu.
† Department of Electrical Engineering and Computer Science.
‡ Department of Chemistry.

(1) Horowitz, G. *Adv. Mater.* **1998**, *10*, 365−377.
(2) Katz, H. E.; Bao, Z. N.; Gilat, S. L. *Acc. Chem. Res* **2001**, *34*, 359−369.
(3) Sirringhaus, H.; Tessler, N.; Friend, R. H. *Science* **1998**, *280*, 1741−1744.
(4) Burroughes, J. H.; Bradley, D. D. C.; Brown, A. R.; Marks, R. N.; Mackay, K.; Friend, R. H.; Burns, P. L.; Holmes, A. B. *Nature* **1990**, *347*, 539−541.
(5) Kovac, J.; Peternai, L.; Lengyel, O. *Thin Solid Films* **2003**, *433*, 22−26. Furuta, P.; Brooks, J.; Thompson, M. E.; Fréchet, J. M. J. *J. Am. Chem. Soc.* **2003**, *125*, 13165−72.
(6) Huynh, W. U.; Dittmer, J. J.; Janke J.; Libby, William C.; Whiting, Gregory L.; Alivisatos, A. P. *Adv. Funct. Mater.* **2003**, *13*, 73−79. Liu, J.; Tanaka, T.; Sivula, K.; Alivisatos, A. P.; Fréchet, J. M. J. *J. Am. Chem. Soc*. **2004**, *126*, 6550−6551.
(7) Crone, B.; Dodabalapur, A.; Gelperin, A.; Torsi, L.; Katz, H. E.; Lovinger, A. J.; Bao, Z. *Appl. Phys. Lett.* **2001**, *78*, 2229−2231.
(8) Someya, T.; Katz, H. E.; Gelperin, A.; Lovinger, A. J.; Dodabalapur, A. *Appl. Phys. Lett.* **2002**, *81*, 3079−3081.
(9) Brown, A. R.; Pomp, A.; Hart, C. M.; Deleeuw, D. M. *Science* **1995**, *270*, 972−974.
(10) Crone, B.; Dodabalapur, A.; Lin, Y. Y.; Filas, R. W.; Bao, Z.; LaDuca, A.; Sarpeshkar, R.; Katz, H. E.; Li, W. *Nature* **2000**, *403*, 521−523.
(11) Drury, C. J.; Mutsaers, C. M. J.; Hart, C. M.; Matters, M.; de Leeuw, D. M. *Appl. Phys. Lett.* **1998**, *73*, 108−110.
(12) Garnier, F.; Hajlaoui, R.; Yassar, A.; Srivastava, P. *Science* **1994**, *265*, 1684−1686.
(13) Rogers, J. A.; Bao, Z.; Meier, M.; Dodabalapur, A.; Schueller, O. J. A.; Whitesides, G. M. *Synth. Met.* **2000**, *115*, 5−11.
(14) Rogers, J. A.; Bao, Z.; Baldwin, K.; Dodabalapur, A.; Crone, B.; Raju, V. R.; Kuck, V.; Katz, H.; Amundson, K.; Ewing, J.; Drzaic, P. *Proc. Natl. Acad. Sci. U.S.A.* **2001**, *98*, 4835−4840.
(15) Sirringhaus, H.; Kawase, T.; Friend, R. H.; Shimoda, T.; Inbasekaran, M.; Wu, W.; Woo, E. P. *Science* **2000**, *290*, 2123-2126.
(16) Speakman, S. P.; Rozenburg, G. G.; Clay, K. J.; Milne, W. I.; Ille, A.; Gardner, I. A.; Bresler, E.; Steinke, J. H. G. *Org. Electron.* **2001**, *2*, 65−73.
(17) Afzali, A.; Breen, T. L.; Kagan, C. R. *Chem. Mater.* **2002**, *14*, 1742−1746.
(18) Garnier, F.; Hajlaoui, R.; El Kassmi, A.; Horowitz, G.; Laigre, L.; Porzio, W.; Armanini, M.; Provasoli, F. *Chem. Mater.* **1998**, *10*, 3334−3339.
(19) Katz, H. E.; Li, W.; Lovinger, A. J.; Laquindanum, J. *Synth. Met.* **1999**, *102*, 897−899.
(20) Sandberg, H.; Henze, O.; Kilbinger, A. F. M.; Sirringhaus, H.; Feast, W. J.; Friend, R. H. *Synth. Met.* **2003**, *137*, 885−886.
(21) Schenning, A. P. H. J.; Kilbinger, A. F. M.; Biscarini, F.; Cavallini, M.; Cooper, H. J.; Derrick, P. J.; Feast, W. J.; Lazzaroni, R.; Leclère, P.; McDonell, L. A.; Meijer, E. W.; Meskers, S. C. J. *J. Am. Chem. Soc.* **2002**, *124*, 1269−1275.

10.1021/cm0496570 CCC: $27.50
Published on Web 08/05/2004

Scheme 1. Thermolysis of Branched α,ω-Ester-Functionalized Sexithiophenes

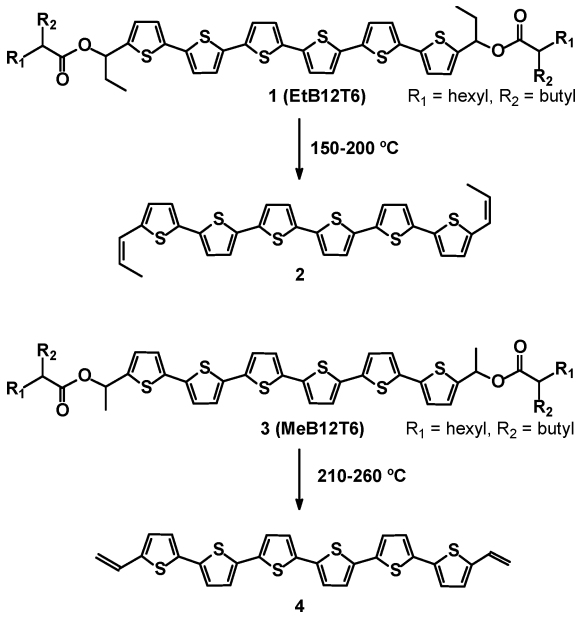

at room temperature. A subsequent heating cycle to induce thermolytic removal of the ester solubilizing groups (affording **2**) permitted the molecules to readopt the preferred π-stacking orientation that resulted in high charge mobility through the material. Device testing of thin film transistors showed an increase in hole mobility from 1×10^{-5} cm^2/V s with on/off ratios of ~100 before thermolysis to 5×10^{-2} cm^2/V s with on/off ratios $> 10^5$ after thermolysis.

The focus of this study is to monitor the effect of processing conditions on the self-assembly of **EtB12T6** and how this morphology effects OTFT performance. Solution deposition methods such as spin-coating, dip-casting and inkjet-printing were optimized for solvent, annealing temperatures, and substrate surface treatment. We also investigated a similar material **MeB12T6** (**3**) that is designed to generate **4** upon thermolysis, leaving terminal vinyl groups that can thermally cross-link. The morphology of the cross-linked films of **4** was compared to the highly mobile films of **2**, and this morphology was, in turn, correlated to device performance.

Results and Discussion

Synthesis and Characterization. EtB12T6 (**1**) was synthesized as previously reported.[22] **MeB12T6** (**3**) was synthesized as shown in Scheme 2. Commercially available 2-acetylthiophene was reduced with $LiAlH_4$ and then esterified using 2-butyloctanoyl chloride to afford **7**. Bromination with NBS, followed by Stille coupling with 5-(tributylstannyl)-2,2′-bithiophene, gave terthiophene **9**. An additional NBS bromination and homocoupling via a Suzuki reaction generated the target **3** as a waxy orange solid.

Thermolysis of **MeB12T6** was monitored using thermogravimetric analysis (TGA) and compared with data from **EtB12T6** (Figure 1). For each compound the loss

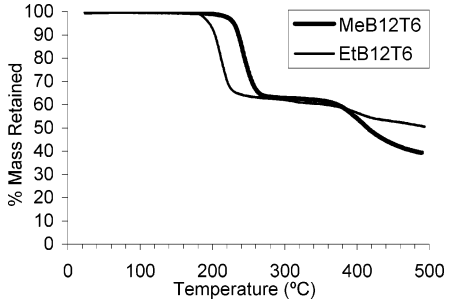

Figure 1. Thermogravimetric analysis of compounds **EtB12T6** and **MeB12T6** heating at 5 °C/min. The onset of decomposition increases from ca. 180 °C for **EtB12T6** to ca. 210 °C for **MeB12T6**.

Scheme 2. Synthesis of MeB12T6

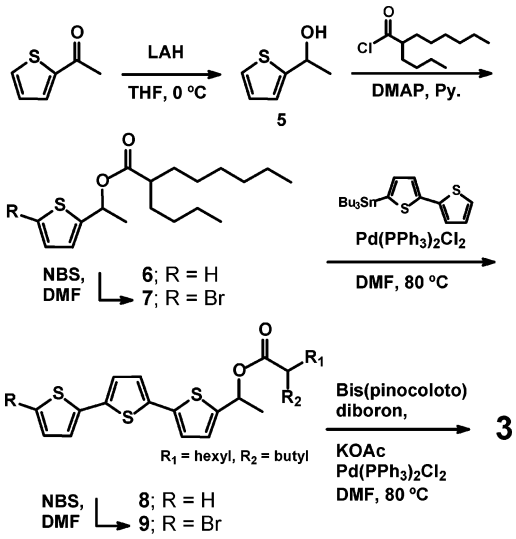

of mass observed upon thermolysis matched that expected from theory (ca. 41%) for the loss of the carboxylic acids, but the onset of decomposition[23] of **MeB12T6** was found to occur at a slightly higher temperature than was measured for **EtB12T6**. MALDI-TOF mass spectrometry of the samples after heating confirmed that **2** and **4** are the only observable thermolysis products of **1** and **3**.

The UV−vis absorptions of **MeB12T6** and **EtB12T6** were also compared. While the absorption spectra of the two compounds were nearly identical in chloroform (λ_{max} = 422 nm) and in the solid state (λ_{max} = 411 nm), the absorption of their respective thermolysis products was strikingly different (Figure 2). In the case of **MeB12T6**, a 45 nm increase in λ_{max} to 457 nm was seen, indicating that the conjugation length is increasing due to the formation of conjugated vinyl groups at either end of the molecule.[24] However, **EtB12T6** showed the opposite trend. After heating, the λ_{max} blue-shifted 25 nm to 384 nm, suggesting an effective conjugation length of four

(22) Murphy, A. R.; Fréchet, J. M. J.; Chang, P.; Lee, J.; Subramanian, V. *J. Am. Chem. Soc.* **2004**, *126*, 1596−1597.

(23) The decomposition temperature is affected markedly by the conditions used to carry out thermolysis, since the process is acid-catalyzed and acid is produced during the thermolysis. In the presence of trace amounts of acid (that may also originate from the solvent used in sample preparation or the surface itself), the decomposition temperature is lowered significantly.

(24) Fujimoto, H.; Nagashima, U.; Inokuchi, H.; Seki, K.; Nakahara, H.; Nakayama, J.; Hoshino, M.; Fukuda, K. *J. Chem. Phys.* **1988**, *89*, 1198−1199. It should be noted here that spontaneous thermal polymerization of **4** can also occur at elevated temperatures.

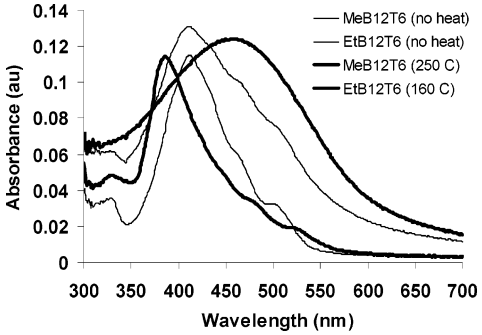

Figure 2. Solid-state UV−vis of **MeB12T6** and **EtB12T6** before and after heating. **MeB12T6** and **EtB12T6** have an initial λ_{max} of 411 nm, which shifts to 457 and 384 nm, respectively, after thermolysis.

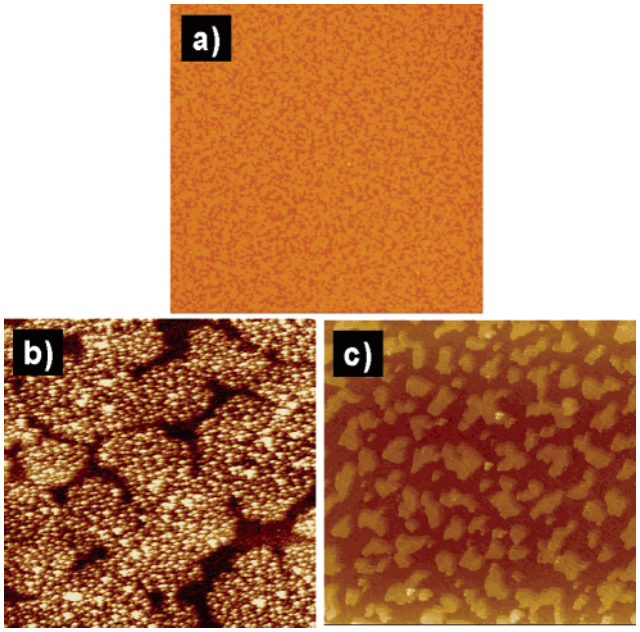

Figure 3. AFM scans of 5 μm × 5 μm areas of thermolyzed films of **EtB12T6** spun cast from (a) 1,2-dichlorobenzene, (b) xylene, and (c) anisole.

thiophene units.[24,25] These data suggest possible disruption in the planarity of the molecule, but the exact nature and extent of this disruption have yet to be determined.

Film Morphology. To investigate the effect of solvent on solution-processed devices of **EtB12T6**, solvents were chosen with boiling points that spanned both the phase transition and decomposition temperatures of the materials. It was expected that the higher boiling solvents would aid in the self-assembly of the molecules during thermolysis and therefore give a more ordered film. However, it was found that regardless of thermolysis time and temperature, films of **EtB12T6** spun-cast from the high-boiling solvents 1,2-dichlorobenzene, anisole, and xylene were discontinuous and amorphous in nature, as imaged by AFM (Figure 3). A range of concentrations and controlled heating/cooling ramps were explored with these solvents, but continuous crystalline films failed to form.

Films of **EtB12T6** spun-cast from chloroform, however, showed the most dramatic change in morphology

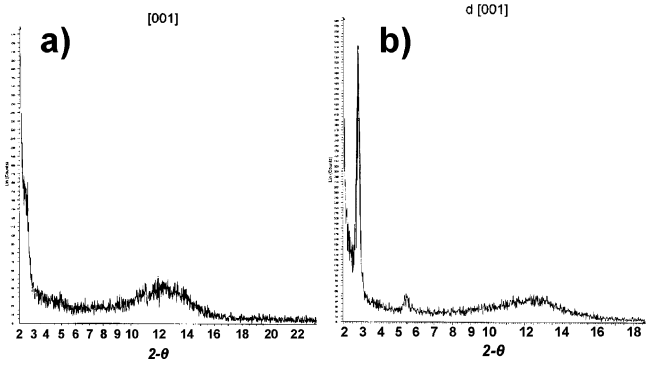

Figure 4. X-ray diffractogram for a film of **EtB12T6** spun from chloroform (a) before heating and (b) after heating to 185 °C. New peaks appear in the thermolyzed sample at 3° and 5.5°.

after heating. AFM performed on thermolyzed films revealed the formation of distinct terraces, with step heights of ∼3.0 nm, corresponding to the expected length of **2**. The crystallinity of these films was evaluated with XRD, which revealed peaks around 3° and 5.5°, where the unheated films exhibited no peaks (Figure 4). Both of the peaks seen in the thermolyzed films are consistent with peaks observed in highly ordered thermally evaporated sexithiophene films.[26,27]

Thermolysis temperature[23] also had a profound effect on the morphology. All thermolyzed samples revealed the formation of molecular terraces that aggregate into regions of vertical growth, similar to that observed for thermally evaporated oligomers.[28] However, at temperatures below 180 °C, larger terraces were covered by smaller aggregates, giving an overall disordered appearance (Figure 5b). As the temperature was increased to 200 °C, the film morphology became dominated by large round terraces on the order of 2−5 μm in diameter and >100 nm high, interspersed within regions of low terraces 3−9 nm high (Figure 5c). Higher temperatures increased the overall height of the terraces, while smaller islands coalesced into larger ones (Figure 5d). The terraced nature of the film led to significant surface roughness (rms ∼ 3 nm), but the regions of the film that seemed to be empty, especially at higher annealing temperatures, in fact appeared to be both crystalline and continuous. High semiconducting behavior further confirmed the presence of at least a monolayer of material in these regions.

The transition from an amorphous, locally aggregated film into one with a high degree of long-range polycrystallinity is notable, particularly at the low temperatures demonstrated. The relatively high surface energy of silicon dioxide with respect to the deposited material likely favored the observed full lateral coverage. This phenomenon is similar to the Stranski−Krastanov growth mode in thin films,[29] where film growth becomes vertical following complete coverage in the lateral direction when the surface energy of the substrate is higher than that of the material being deposited.

(25) Becker, R. S.; Demelo, J. S.; Macanita, A. L.; Elisei, F. *Pure Appl. Chem.* **1995**, *67*, 9−16.

(26) Lang, P.; Hajlaoui, R.; Garnier, F.; Desbat, B.; Buffeteau, T.; Horowitz, G.; Yassar, A. *J. Phys. Chem.* **1995**, *99*, 5492−5499.

(27) Garnier, F.; Yassar, A.; Hajlaoui, R.; Horowitz, G.; Deloffre, F.; Servet, B.; Ries, S.; Alnot, P. *J. Am. Chem. Soc.* **1993**, *115*, 8716−8721.

(28) Müller, E.; Ziegler, C. *J. Mater. Chem.* **2000**, *10*, 47−53.

(29) Bauer, E. *Z. Kristallogr.* **1958**, 372.

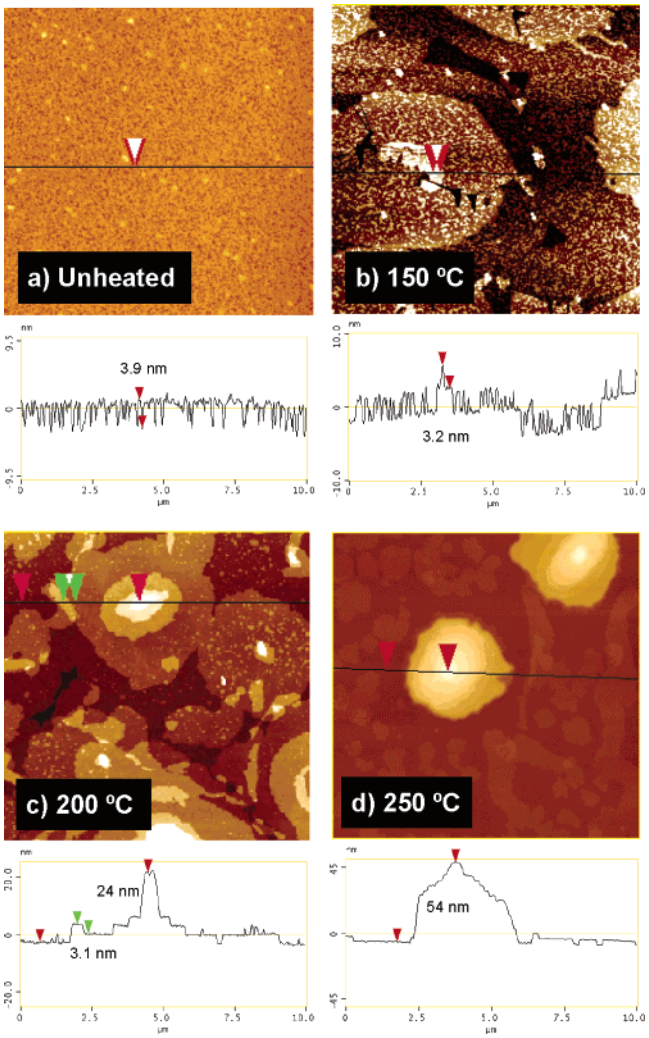

Figure 5. 10 μm × 10 μm AFM images and height profiles of **EtB12T6** films spun-cast from chloroform and then heated for 20 min at the indicated temperatures.

To investigate the role of substrate surface energy on film morphology, different dielectric surfaces were tested. Hydrophobic organic surfaces with a high contact angle have been shown to enhance performance in OTFTs.[3,30] While the mechanism for mobility enhancement is not clear, it is often attributed to a passivation of a highly polar surface that otherwise would have a profound impact on the orientation of the first deposited monolayer. With a more hydrophobic surface, the intermolecular attraction between conjugated molecules becomes the dominant ordering mechanism during film growth.

Octadecyltrichlorosilane (OTS) was self-assembled on silicon dioxide to provide a hydrophobic, low surface energy interface between the substrate and the semiconducting oligomers.[31,32] **EtB12T6** was spun cast from chloroform onto the OTS, resulting in a visually rough film after heat treatment. AFM images confirmed the formation of a discontinuous film consisting of round aggregates dispersed on top of the OTS, up to 4 μm in diameter and 500 nm in height (Figure 6a). Higher resolution scans revealed scattered terraces 3−6 nm in height between the larger aggregates. These terraced areas covered less than 10% of the substrate surface, with the bulk of the deposited material contained in the large spherical aggregates. Films processed by dip-casting resulted in the same discontinuous morphology.

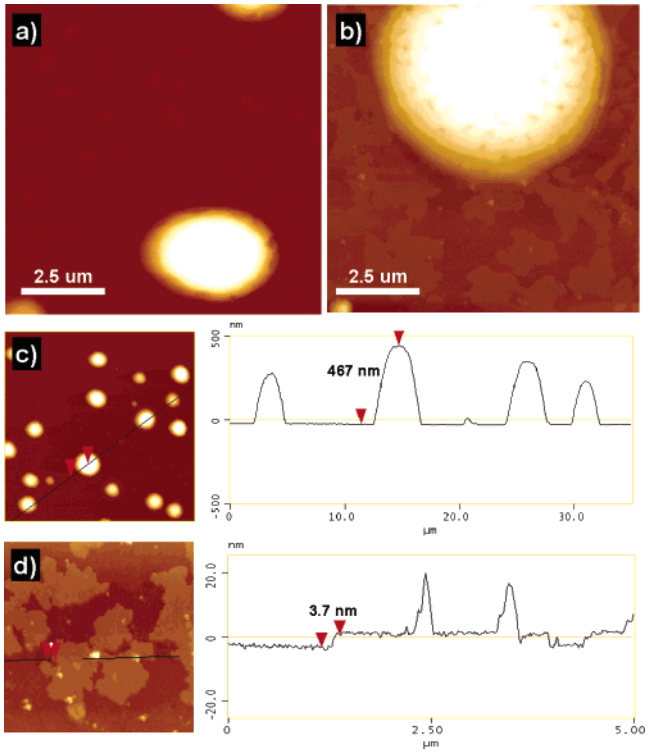

Figure 6. AFM scans of a heated film of **EtB12T6** on (a) OTS- and (b) PVP-treated silicon. Both show large aggregated regions. (c) 35 μm scan and cross-section of a heated film on a PVP-treated surface, showing aggregate heights of over 500 nm dispersed across the surface. (d) 5 μm scan of the area between the large aggregates of PVP revealing the presence of monolayer thick terraces.

Further surface treatment studies were performed with poly(vinylphenol) (PVP), an organic dielectric that has been previously shown to be effective in OTFTs with other small molecules.[31,33,34] As with OTS-treated substrates, films prepared on PVP-coated silicon wafers were discontinuous with large circular aggregates over 300 nm in height dispersed between low level terraces one or two monolayers thick (Figure 6b−d). The low level terraces seemed to exhibit a high void density with <50% coverage but exhibited significantly more coverage than in the OTS-treated samples.

A final comparison was performed with SiO_2 substrates treated with hexamethyldisilizane (HMDS). With a contact angle of 80°, the surface energy is between that of untreated silicon dioxide and OTS-treated oxide. Continuous films with clear terracing were observed on HMDS-coated substrates, although total feature height appeared larger with visible aggregation when compared to bare oxide samples treated at equal temperatures (Figure 7).

(30) Sirringhaus, H.; Tessler, N.; Friend, R. H. *Synth. Met.* **1999**, *102*, 857−860.
(31) Halik, M.; Klauk, H.; Zschieschang, U.; Schmid, G.; Ponomarenko, S.; Kirchmeyer, S.; Weber, W. *Adv. Mater.* **2003**, *15*, 917−923.
(32) Bao, Z. N.; Kuck, V.; Rogers, J. A.; Paczkowski, M. A. *Adv. Funct. Mater.* **2002**, *12*, 526−531.
(33) Klauk, H.; Halik, M.; Zschieschang, U.; Schmid, G.; Radlik, W.; Weber, W. *J. Appl. Phys.* **2002**, *92*, 5259−5263.
(34) Collet, J.; Tharaud, O.; Chapoton, A.; Vuillaume, D. *Appl. Phys. Lett.* **2000**, *76*, 1941−1943.

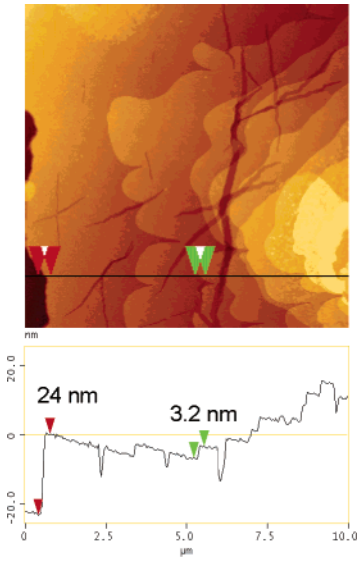

Figure 7. 10 μm × 10 μm AFM scan and height profile of a heated film of **EtB12T6** on HMDS-treated SiO_2. Clear molecular terracing is seen but in much larger aggregates than on bare SiO_2.

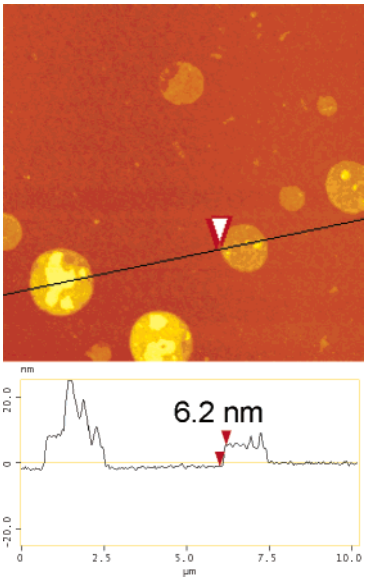

Figure 8. AFM image and cross-section of a film of **MeB12T6** on SiO_2 annealed at 200 °C.

In the case of OTS- and PVP-treated SiO_2, the hydrophobic organic surface treatment failed to produce the continuous, crystalline films observed on bare SiO_2. The surface energy of the organic substrates was likely lowered to the point where it was no longer energetically favorable for molecules of **EtB12T6** to spread evenly on the surface, leading instead to the formation of large aggregates with little overall surface coverage. This conclusion was further verified using the intermediate hydrophobicity surface treatment HMDS. The crystallinity of the resulting films was closer to that seen on bare SiO_2, but a larger degree of aggregation was observed. Therefore, it appears that a substrate of adequate surface energy is required in order to obtain full lateral coverage.

The large amount of rearrangement observed in thermolyzed films of **EtB12T6** on hydrophobic surfaces led us to investigate the effect of restraining this movement. **MeB12T6** was spun-cast from chloroform onto a SiO_2 substrate, generating films with morphology and thickness similar to that of unheated films of **EtB12T6**. These films were then subjected to a range of annealing temperatures between 190 and 260 °C to see if any trends similar to those seen in the **EtB12T6** films could be observed. While all samples cast from chloroform were continuous, the majority of the films of **MeB12T6** imaged by AFM appeared amorphous in nature, independent of annealing temperature. Although some samples exhibited aggregation in the form of islandlike growth, the primary step height seen was on the order of 6 nm, which is roughly twice the expected height of a single monolayer. (Figure 8). Also, no diffraction peaks could be detected by XRD analysis, further verifying the amorphous nature of the films.

The ability of **MeB12T6** to thermally cross-link at the annealing temperatures applied can restrict the movement of the molecules on a surface, potentially leading to more robust films. However, the fact that most of the films of **MeB12T6** remain amorphous after thermolysis suggests that much of the organization seen in films of **2** takes place after thermolysis, and no pre-ordering of the branched oligomers occurs. Therefore, the possible restriction of movement by partial or full cross-linking of **4** leads to films with poor ordering.

Although spin-casting often offers the most reproducible set of processing conditions, dip-casting typically leads to highest performance in solution-processed OTFTs.[35] To compare these processes, several thin films of **EtB12T6** were dip-cast using chloroform or anisole as the solvent. While films of varying thickness were deposited due to uneven solvent evaporation, morphology following heat treatment was similar to that seen in spun-cast films, as imaged by AFM. It is notable that dip-cast films from anisole exhibited significantly higher coverage than those formed by spin-casting. Therefore, it is likely that further work aimed at refining spin-casting conditions for solvents such as xylene and anisole could lead to full coverage of **EtB12T6** films.

Further investigation into the compatibility of **EtB12T6** with additive print-based patterning was also explored. Devices were printed from solution via a piezo-driven inkjet-printing process. While chloroform was found to be the optimal solvent for spin-casting, anisole was chosen as the printing solvent due to ease of integration with existing inkjet processes. A range from 1 to 32 drops of **EtB12T6** in anisole was ink-jetted onto SiO_2 containing prepatterned gold electrodes and then heated under nitrogen at 190 °C for 30 min.

When examined by AFM, molecular terraces similar to those found in films spun from chloroform were observed for films with less than four drops. Coverage tended to be partial in devices with large dimensions with a channel length of >10 μm, but films were essentially void free when measured between adjacent source and drain electrodes in devices with a channel length of 5 μm. This was in sharp contrast to the films spun from anisole under the same concentration, where films were highly discontinuous with <50% coverage. Multidrop devices showed nearly full coverage, with the level of terracing increasing with the number of printed

(35) Bao, Z. N.; Dodabalapur, A.; Lovinger, A. J. *Appl. Phys. Lett.* **1996**, *69*, 4108−4110.

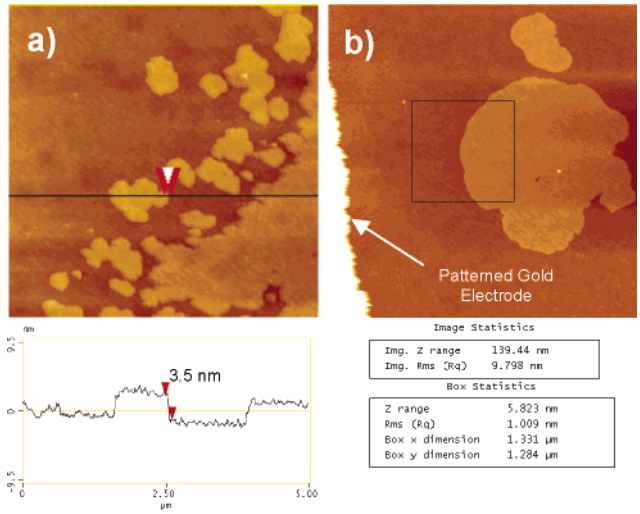

Figure 9. AFM scans of ink jetted films. (a) Height profile of a multidrop film of **EtB12T6** with terraces similar to that seen in spun cast films. (b) Scans within the channel show a film rms roughness of 0.3 nm, with a maximum height of 6 nm within the scan.

drops (Figure 9a). Overall, all measured films showed a characteristic rms value of ~0.3 nm, with the maximum *Z*-range values in multiples of ~3 nm (Figure 9b). The exceptionally low surface roughness across large area scans revealed what appeared qualitatively to be a lack of grain boundaries, which was not clearly apparent in the highly terraced films spun from chloroform.

Device Performance. OTFT devices were fabricated on low-resistivity n-type silicon wafers, using thermally grown silicon dioxide as the dielectric, unless otherwise noted, in either top- or bottom-contact geometries. The active semiconducting layer was then applied by the solution-deposition methods discussed above. All devices were tested as p-type OTFTs in the accumulation regime and saturation mobilities were calculated using the equation $\mu = gm^2/2I_DC_{ox}(W/L)$. Various shadow masks were used for the top contact devices, giving channel lengths from 5 to 100 μm. The lower end of the channel lengths gave device sizes with dimensions on the order of single terrace features, but measured performance was consistent with conventional device scaling, and no preferential effects were observed as channel length spanned regions on the order of single aggregated grains.

The best device results for each of these processes are summarized in Table 1 for **EtB12T6**. These results were found to correlate well with the observed film morphologies, where the most ordered, crystalline films gave the highest mobilities. All top contact devices tested prior to heat treatment for these samples yielded low field-effect mobilities in the range of 10^{-5} cm^2/V s with on/off ratios from 10 to 100.

The hole mobilities through top-contact devices made from spun-cast films from 1,2-dichlorobenzene and anisole were low, as expected from the poor film continuity. Thin films spun-cast from xylene, however, exhibited an increase in field-effect mobility by a factor of 10−100, with a corresponding increase in on/off ratio. Similarly, devices using OTS-treated SiO_2 as the dielectric had low mobilities, regardless of solvent. Devices

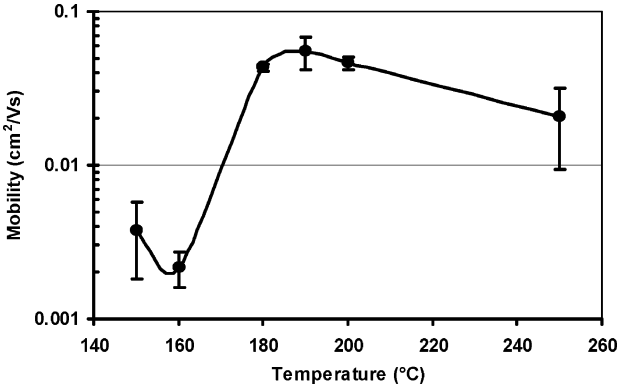

Figure 10. Measured mobility vs annealing temperature in devices of **EtB12T6** spun-cast from chloroform.

Table 1. Peak Measured Mobilities of EtB12T6 for the Given Deposition Methods

device structure	solvent	μ_{max} (cm^2/V s)	on/off
	Spin-Casting		
top contact, SiO_2	chloroform	0.07	10^5
	xylene	0.005	10^3
	1,2-dichlorobenzene	<0.0001	-
	anisole	<0.0001	-
top contact, OTS	chloroform	<0.0001	-
	xylene	<0.0001	-
top contact, PVP	chloroform	0.0006	10^3
	Dip-Casting		
top contact, SiO_2	chloroform	0.04	10^5
	anisole	0.02	10^4
bottom contact, SiO_2	chloroform	0.04	10^5
	anisole	0.002	10^4
	Inkjet-Printing		
bottom contact, SiO_2	anisole	0.06	10^8

using the organic dielectric PVP had an order of magnitude improvement over the OTS-treated devices, even though the film morphologies appeared similar. The higher observed coverage of **EtB12T6** on the PVP film is likely the cause for the relative increase in measured current. While the aggregate diameters were also larger on the PVP, and in many cases completely spanned the channel between electrodes, this was not apparent in all devices that exhibited semiconducting behavior.

More extensive device testing was done using films spun-cast from chloroform, which had the most crystalline morphology. The highest measured mobility in multiple top-contact devices was >0.07 cm^2/V s with an on/off ratio > 10^5. Devices annealed at temperatures between 150 and 250 °C were tested at various intervals, and heating duration was varied logarithmically from 2 to 500 min in factors of 5. While thermolysis[23] of **EtB12T6** could be completed at 170 °C, the peak performance in tested OTFTs was not found to occur until 180 °C and above (Figure 10). Above 180 °C, device performance remained consistent through 200 °C and then began to slowly degrade from 200 to 250 °C. Peak mobilities were also found to occur when the devices were heated between 10 and 20 min. Samples heated for 500 min under dry nitrogen did not show consistently higher performance than samples heated for 20 min. Samples with ramped heating exhibited slightly degraded performance when compared with samples heated to the same final temperature, while samples

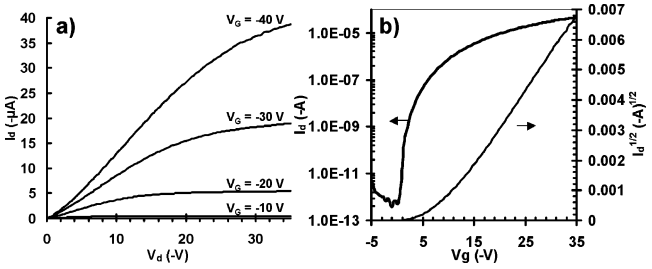

Figure 11. Electrical characterization of inkjet-printed OTFTs after heating to 190 °C. (a) Drain current I_D vs drain voltage V_D as a function of gate voltage for a top-contact device with $L = 300$ μm and $W = 4$ μm. (b) I_D and $I_D^{1/2}$ vs V_G at $V_D = -35$ V.

with ramped cooling performed similar to the same control samples.

Devices constructed by dip-casting solutions of **EtB12T6** in anisole yielded top-contact devices with a measured mobility of 0.022 cm^2/V s. In bottom-contact devices, the highest measured mobility was 0.002 cm^2/V s, although performance varied widely, depending on region tested. Dip-cast devices using chloroform solutions at dilute concentrations of 1.5 mg/mL led to regions of devices performing near that observed in spun-cast samples, with mobilities as high as 0.043 cm^2/V s. However, higher concentration solutions led to lower mobility. Dip casting was also performed with prepatterned bottom-contact devices, with measured mobilities as high as 0.034 cm^2/V s. Similar to bottom-contact devices from films deposited using small molecule evaporation, visible contact resistance was observable. While performance in the bottom contact devices was slightly lower than that seen in top contact, this difference was less than the factor of 2−3 typically observed in evaporated devices.[31,36]

Multidrop ink-jetted devices exhibited mobilities as high as 0.06 cm^2/V s, with an average mobility of 0.05 cm^2/V s (Figure 11). The on/off ratios of $>10^8$ were significantly superior to those of spun-cast films due to better device isolation made possible with printing. Overall, it is notable that the field-effect mobility in these bottom-contact devices nearly matched that measured in the spun-cast top-contact devices. As top-contact devices typically perform 2−3 times better,[3,31,36] this may suggest that further thin film optimization can lead to increased performance.

Devices fabricated using **MeB12T6** failed to exhibit a significant increase in field-effect mobility following applied temperatures from 200 to 275 °C. Unheated films did not show significant semiconducting behavior with mobilities $<10^{-5}$ cm^2/V s, while heated films exhibited a slightly increased gate modulation resulting in mobilities $\sim 10^{-4}$ cm^2/V s. Interestingly, select devices within the identical sample also exhibited significant off current densities 10^3 higher than both other devices on the same sample and devices fabricated using **EtB12T6**. Attempts to image any particular aggregation responsible for this higher conductivity failed to find differences resolvable by AFM. Overall, it is notable that a slight change in the end termination of an oligothiophene led to the formation of dramatically different films with different electrical characteristics.

Conclusion

Oligothiophenes containing thermally labile solubilizing groups were cast into thin films by various solution processes. A low-temperature heat treatment was used to remove the bulky ester groups by thermolysis, thus allowing the materials to self-assemble into highly crystalline thin films with visible molecular terracing. Variation of solvents, process conditions, and casting technique optimized both the morphology and electrical performance of the films. Fabricated OTFTs using **EtB12T6** exhibited a dramatic increase in performance following conversion, with field-effect mobilities approaching 0.08 cm^2/V s and on/off ratios $> 10^8$. However, alterations to the terminal substituents of the molecule dramatically altered the film formation and the corresponding electrical performance. Such results highlight the challenges in developing novel materials combining solution processability with thin film crystallinity.

Alternative dielectric surfaces were investigated, with the ultimate goal of a fully solution cast process. Used in conjunction with demonstrated nanoparticle metals[37] and soluble organic semiconductors, soluble dielectrics may allow for fully solution processed thin film transistors. Films cast on organic surfaces, however, demonstrated potential challenges in achieving compatibility with low surface energy organic interfaces. While results were still significantly lower than on silicon dioxide, the common organic dielectric PVP showed promise in allowing the formation of crystalline films exhibiting some semiconducting properties.

Finally, inkjet printing was used to deposit the active semiconducting layer on top of lithographically patterned electrodes. The resulting films were crystalline in nature, similar to those observed in spun-cast films. Peak electrical performance, with mobilities as high as 0.06 cm^2/V s with on/off ratios $> 10^8$, approached that measured in top-contact devices. Although device variation was high, the impressive quality of several films demonstrates the potential for print based processes for depositing crystalline films. The strong self-organizing nature of these thiophene oligomers shows promise as a critical component in the creation of fully printed circuits.

Acknowledgment. We thank the AFOSR, DOE-BES, NSF, the Eastman-Kodak Co., and MARCO for funding.

Supporting Information Available: Complete experimental procedures and characterization of **3**−**8** and all OTFT fabrication procedures (PDF). This material is available free of charge via the Internet at http://pubs.acs.org.

CM0496570

(36) Dimitrakopoulos, C. D.; Malenfant, P. R. L. *Adv. Mater.* **2002**, *14*, 99.

(37) Huang, D.; Liao, F.; Molesa, S.; Redinger, D.; Subramanian, V. *J. Electrochem. Soc.* **2003**, *150*, G412-G417.